Mass and size effects in three-dimensional vibrofluidized granular mixtures

Peter E. Krouskop and Julian Talbot*
Department of Chemistry and Biochemistry, Duquesne University, Pittsburgh, Pennsylvania 15282-1530, USA
(Received 13 March 2003; published 27 August 2003)

We examine the steady state properties of binary systems of driven inelastic hard spheres. The spheres, which move under the influence of gravity, are contained in a vertical cylinder with a vibrating base. We computed the trajectories of the spheres using an event-driven molecular dynamics algorithm. In the first part of the study, we chose simulation parameters that match those of experiments published by Wildman and Parker. Various properties computed from the simulation including the density profile, granular temperature, and circulation pattern are in good qualitative agreement with the experiments. We then studied the effect of varying the mass ratio and the size ratio independently while holding the other parameters constant. The mass and size ratio are shown to affect the distribution of the energy. The changes in the energy distributions affect the packing fraction and temperature of each component. The temperature of the heavier component has a nonlinear dependence on the mass of the lighter component, while the temperature of the lighter component is approximately proportional to its mass. The temperature of both components is inversely dependent on the size of the smaller component.

DOI: 10.1103/PhysRevE.68.021304 PACS number(s): 45.70.Mg, 47.20.Bp, 47.27.Te, 81.05.Rm

I. INTRODUCTION

Granular systems exhibit many properties that are different from systems composed of elastic particles. For example, driven granular systems display standing and traveling waves [1–3], oscillons [4], heaping, and convection [5,6]. In addition, granular mixtures show size segregation [7] and steady-state kinetic energies that are not equal for each component in the mixture [8]. This departure from equipartition is not unexpected, but it is one of the most striking differences between elastic and inelastic systems. Understanding the properties of mixtures is particularly important for granular systems since, unlike molecular systems, they are never completely monodisperse.

Theoretical studies of granular systems have focused on two distinct classes. One consists of systems that are not driven or heated. The initial energy decays over time as a result of inelastic collisions. During this ''cooling'' process there is a period during which the density is homogeneous. Several workers have presented kinetic theories [9–11] and mean-field theories based on Maxwell models [12] to describe the properties of mixed granular systems in this homogenous cooling state. In the other class of systems, an energy source, such as a vibrating wall, is present. This leads to a nonequilibrium steady state that has been studied by several researchers [9,13–15]. In both classes the components are predicted to have different kinetic energies, or granular temperatures, that depend on the mass, size, and restitution coefficient of the grains [11,14].

Recently, two-dimensional [16] and three-dimensional systems [8,17] of driven, granular mixtures have been studied experimentally. Losert *et al.*, who first reported the difference in granular temperature [8], observed that the velocity distributions deviated from those observed in systems with elastic collisions. Feitosa and Menon studied density distributions and granular temperature profiles in two-dimensional systems with and without gravity [16]. Wildman and Parker have studied the convection patterns, density distributions, and temperature profiles in three-dimensional systems [17]. These studies determined that the heavier particles are at a higher granular temperature than the lighter particles. In both two and three-dimensional systems, the ratio of the temperatures varies as the relative proportion of the heavy and light particles is changed. The temperature ratio, however, is independent of the inelasticity of the particles [16,17].

While the experimental techniques employed in the studies cited above have provided many useful insights into granular behavior, they cannot easily isolate the effects of particle mass, size, and inelasticity. Theoretical and computational methods are useful in this respect. Molecular dynamics simulations of granular mixtures can accurately reproduce the phenomena observed in experiment [18,19], while providing information on the effects of the individual properties mentioned above. For example, Pöschel *et al.* have studied the requirements for the onset of fluidization in a one-dimensional column of beads [20]. Also, Paolotti *et al.* [19] and Barrat and Trizac [21] investigated the effects of rotation, mass ratio, and relative density in two-dimensional vibrated systems. Mixtures have been studied in two-dimensional systems with gravity and a vibrating wall [22] and also under shear flow conditions [23]. Gallas *et al.* used a three-dimensional simulation to study size segregation in mixtures [24]. Equally, simulations of the homogeneous cooling state in two-dimensional systems are consistent with experiment and theory [1,21,23].

It is important to stress that the conclusions drawn from simulations of two-dimensional systems cannot necessarily be extended to three dimensions. In particular, the system boundaries have a much larger influence in three dimensions, as recently demonstrated by Talbot and Viot [18].

This paper presents a three-dimensional, event-driven,

*Author to whom correspondence should be addressed. Email address: talbot@duq.edu

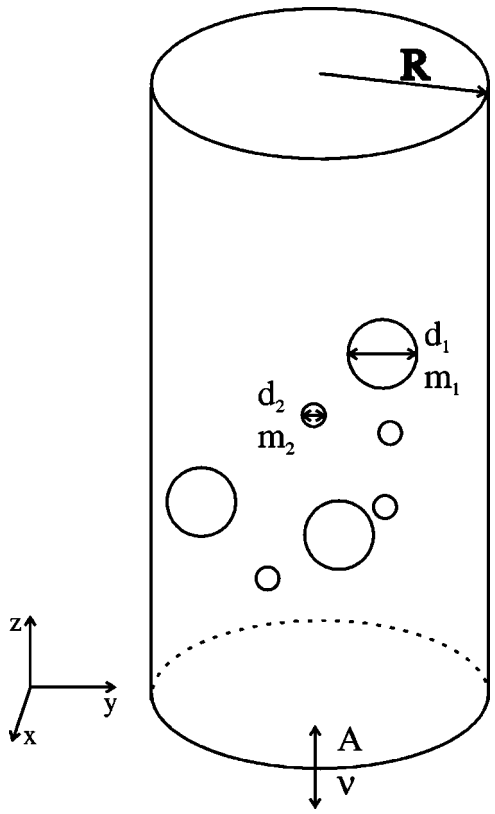

FIG. 1. The three-dimensional system consisting of an infinitely tall cylinder of radius R, and a mixture of hard spheres with sizes d_1 and d_2 and masses m_1 and m_2. The base of the cylinder is shaken with a symmetric sawtooth wave form with amplitude A and frequency ν.

molecular dynamics simulation of a mixture of inelastic hard spheres. The simulation methodology is discussed in Sec. II followed by a comparison to the available experimental results, Sec. III A. Finally, the effects of isolated changes in the mass ratio (Sec. III B) and size ratio (Sec. III C) on the energy distribution and component temperatures are examined.

II. MODEL AND SIMULATION

The three-dimensional system [18] (Fig. 1) contains a mixture of inelastic hard spheres in an infinitely tall cylinder of radius R under the influence of gravity. The mixture is composed of n_1 spheres of mass m_1 and diameter d_1 and n_2 spheres of mass m_2 and diameter d_2. Energy is injected into the system by means of the base of the cylinder, which vibrates in a symmetric saw tooth wave form of amplitude A and frequency ν. This wave form is used in the simulation for modeling simplicity. We do not believe that there is any strong dependence of the system response on the kind of symmetric wave form used to drive the system [25].

Three kinds of collisions occur in the system: particle-particle, particle-wall, and particle-base. The postcollisional velocities ($\mathbf{v}'_{\alpha,\mathbf{i}}$ and $\mathbf{v}'_{\beta,\mathbf{j}}$) resulting from a collision between a particle from component α and a particle from component β with masses m_α and m_β and initial velocities $\mathbf{v}_{\alpha,\mathbf{i}}$ and $\mathbf{v}_{\beta,\mathbf{j}}$, respectively, are given by

$$\mathbf{v}'_{\alpha,\mathbf{i}} = \mathbf{v}_{\alpha,\mathbf{i}} - \frac{m_\beta}{m_\alpha + m_\beta}(1+c)[(\mathbf{v}_{\alpha,\mathbf{i}} - \mathbf{v}_{\beta,\mathbf{j}})\cdot\hat{\mathbf{n}}]\hat{\mathbf{n}}, \quad (1a)$$

$$\mathbf{v}'_{\beta,\mathbf{j}} = \mathbf{v}_{\beta,\mathbf{j}} + \frac{m_\alpha}{m_\alpha + m_\beta}(1+c)[(\mathbf{v}_{\alpha,\mathbf{i}} - \mathbf{v}_{\beta,\mathbf{j}})\cdot\hat{\mathbf{n}}]\hat{\mathbf{n}}. \quad (1b)$$

The unit vector between the centers of the colliding particles is $\hat{\mathbf{n}}$, and c is the appropriate restitution coefficient. While Eqs. (1a) and (1b) conserve momentum, they imply an energy loss of

$$\Delta E = -\frac{1}{2}\mu(1-c^2)[(\mathbf{v}_{\alpha,\mathbf{i}} - \mathbf{v}_{\beta,\mathbf{j}})\cdot\hat{\mathbf{n}}]^2, \quad (2)$$

where $\mu = m_\alpha m_\beta/(m_\alpha + m_\beta)$ is the reduced mass of the particles involved in the collision.

In a binary mixture it is generally necessary to specify three restitution coefficients for particle-particle collisions: c_{11} and c_{22} for intracomponent collisions and $c_{12}(=c_{21})$ for intercomponent collisions. Several authors have reported on random [15,26] and velocity-dependent [27,28] restitution coefficients. Luding and McNamara have proposed a contact time model that also leads to a variable restitution coefficient [29]. For simplicity, we have chosen to use a constant value for the restitution coefficients. We further assume that $c_{11} = c_{22} = c_{12} = c$.

Particle-wall collisions are governed by

$$\mathbf{v}'_{\alpha,\mathbf{i}} = \mathbf{v}_{\alpha,\mathbf{i}} - (1+c_{\alpha,w})(\mathbf{v}_{\alpha,\mathbf{i}}\cdot\hat{\mathbf{r}})\hat{\mathbf{r}}, \quad (3)$$

where $c_{\alpha,w}$ is the appropriate restitution coefficient for component α, and $\hat{\mathbf{r}}$ is the radial unit vector. We assume that the restitution coefficient for collision with the wall is constant for both species and $c_{1,w} = c_{2,w} = c_w$. Particle-base collisions are governed by

$$\mathbf{v}'_{\alpha,\mathbf{i}} = \mathbf{v}_{\alpha,\mathbf{i}} - (1+c_{\alpha,b})[(\mathbf{v}_{\alpha,\mathbf{i}} - \mathbf{v}_{\mathbf{w}})\cdot\hat{\mathbf{k}}]\hat{\mathbf{k}}, \quad (4)$$

where $c_{\alpha,b}$ is the appropriate restitution coefficient for component α, $\mathbf{v}_{\mathbf{w}}$ is the velocity of the base at the instant of collision, and $\hat{\mathbf{k}}$ is the unit vector in the z direction. The restitution coefficients for collisions with the base are also assumed to be constant and equal for both species (i.e., $c_{1,b} = c_{2,b} = c_b$).

A phenomenon similar to inelastic collapse can be observed in these simulations. For certain ranges of the velocity a given particle will collide repeatedly with the side wall. As its energy is dissipated, the particle approaches the wall ever more closely. This is accompanied by an increase in collision frequency that eventually ''freezes'' the simulation. To prevent this phenomenon from occurring, a small impulse is imparted to the particle toward the center of the cylinder once its radial velocity falls below a certain value. This method has been used previously [18], and the threshold value was set such that the injected energy does not discernibly influence the simulation output. It is also possible for a particle to come to rest on the base for a time corresponding to 1/2 a cycle of the vibration. To avoid this possibility, the

sign of the z component of the velocity for the particle is inverted when the velocity of the colliding particle is found to match the velocity of the base. This condition was found to occur once every 12.5×10^6 collisions for the parameter values used in this paper. Thus, this method causes little perturbation in the simulation output.

We calculated a number of properties from the particle positions and velocities generated by the simulation. The packing fraction η_α for component α is defined as

$$\eta_\alpha = \frac{n_\alpha v_\alpha}{V}, \tag{5}$$

where n_α is the number of particles of component α in the volume element V, and $v_\alpha = \pi d_\alpha^3/6$ is the volume of a particle of this component. Another property that we calculated is the kinetic energy or granular temperature T_α of each component using the following equations:

$$T_{\alpha,x} = m_\alpha \langle v_{\alpha,x}^2 \rangle,$$

$$T_{\alpha,y} = m_\alpha \langle v_{\alpha,y}^2 \rangle, \tag{6a}$$

$$T_{\alpha,z} = m_\alpha \langle v_{\alpha,z}^2 \rangle,$$

$$T_\alpha = \frac{(T_{\alpha,x}+T_{\alpha,y}+T_{\alpha,z})}{3} = \frac{m_\alpha \langle v_\alpha^2 \rangle}{3}. \tag{6b}$$

The ''partial'' temperatures in the x, y, and z directions are $T_{\alpha,x}$, $T_{\alpha,y}$, $T_{\alpha,z}$, and the angular brackets denote a time average over all particles of component α.

Our first objective was to model the experimental system studied by Wildman and Parker [17]. We chose simulation parameters that correspond to those of the experiment, i.e., a cylinder of diameter 145 mm that is shaken at 50 Hz with an amplitude of 1.74 mm. The acceleration due to gravity is taken as $g = 9.81$ m/s^2. The restitution coefficient for particle-particle collisions is $c = 0.91$, for particle-wall collisions $c_w = 0.68$, and for particle-base collisions $c_b = 0.88$.

We performed simulations in which we varied the relative proportions of large and small particles while maintaining enough particles to cover the base of the cylinder with a monolayer for comparison to the experimental work of Wildman and Parker [17]. We then performed additional simulations to examine the effect of varying the mass ratio m_2/m_1 and the size ratio d_2/d_1 independently. In the discussion of these three studies, component 2 will always refer to the smaller and/or lighter component.

The particles of each component were randomly placed in the cylinder with random velocities. We then equilibrated all systems for approximately 5000 collisions per particle. Data were collected over 2.4×10^4 collisions per particle at intervals of approximately ten collisions per particle. These data were then averaged for each component to obtain a representation of the system at steady state.

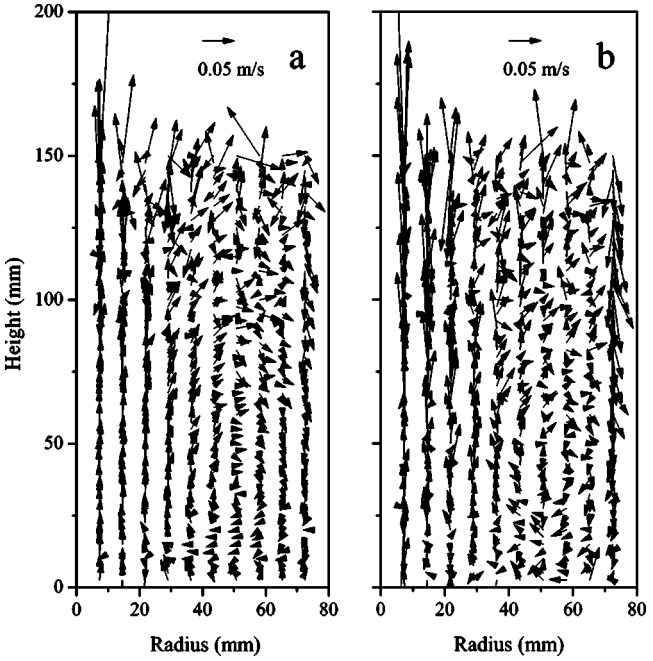

FIG. 2. Velocity field of (a) component 1 and (b) component 2. Simulation conditions as follows: $n_1 = 525$, $n_2 = 270$, $d_2/d_1 = 0.8$, $m_2/m_1 = 0.512$, all other conditions as given in the text.

III. RESULTS AND DISCUSSION

A. Systems with varying composition

For the simulations discussed in this section, the size ratio of the two components was set at $d_2/d_1 = 0.8$ and the mass ratio was set at $m_2/m_1 = 0.512$. Systems with the following compositions were then studied: $n_1 = 525$, $n_2 = 270$; $n_1 = 350$, $n_2 = 540$; and $n_1 = 175$, $n_2 = 810$.

1. Velocity field

The velocity fields of components 1 and 2 for a system with $n_1 = 525$ and $n_2 = 270$ particles are shown in Figs. 2(a) and 2(b), respectively. It can be seen that both components circulate in a pattern that rises in the center of the cylinder and falls at the walls. This convection pattern has been observed previously in both experiment and simulation [17,18,30]. The patterns shown here are very similar to those reported by Wildman and Parker [17] with the center of the convection for both species present at a radius of approximately 50 mm and a height of approximately 40 mm.

2. Packing fraction

The packing fraction, as a function of radius and height for each component, is shown in Fig. 3. It can be seen that there is a density gradient in both the radial and vertical directions for both components, just as is observed in monodisperse systems [18,30]. The data from the simulation are qualitatively similar to those observed in experiment, except that the simulation shows a higher concentration at the bottom of the cylinder near the wall for both components. It should be noted that while the maximum density occurs at the same point for both components, component 2 obtains a

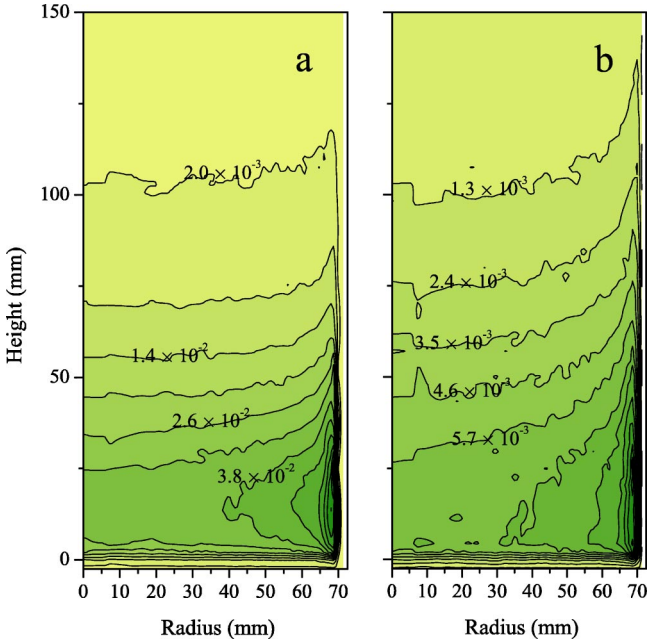

FIG. 3. (Color online) Contour plots of the packing fraction of (a) component 1 and (b) component 2. Contours correspond to a packing fraction change of 0.006 in (a) and 0.0011 in (b). Simulation conditions as given in Fig. 2.

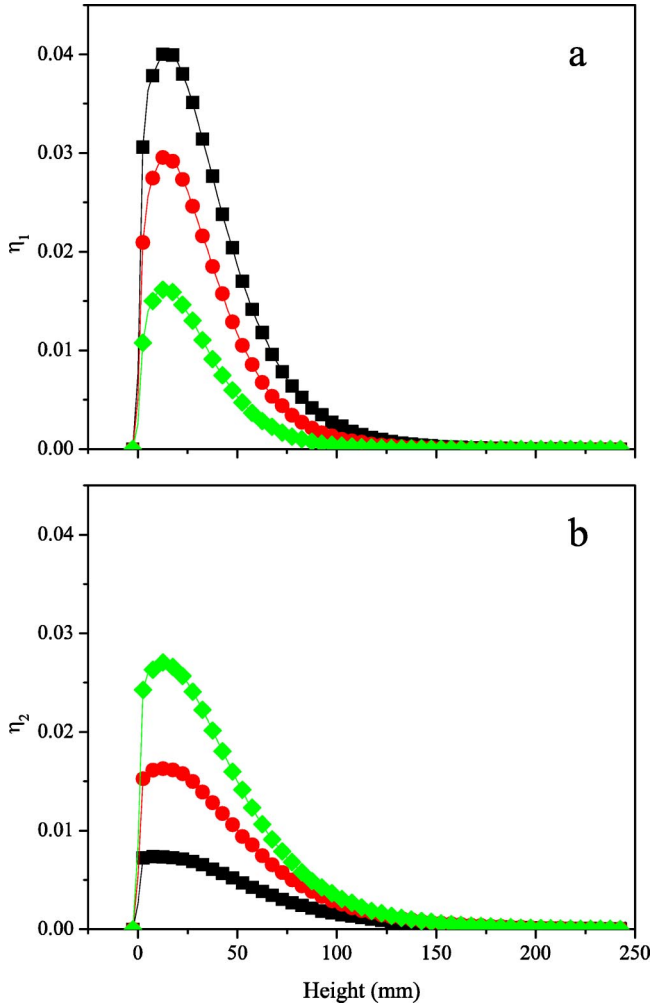

FIG. 4. (Color online) Packing fractions of (a) component 1 and (b) component 2 for the compositions: ■, $n_1=525$, $n_2=270$; ●, $n_1=350$, $n_2=540$; ◆, $n_1=175$, $n_2=810$. Other simulation conditions as given in Fig. 2.

greater height than component 1. This trend is opposite to that observed for size segregation in weakly tapped systems where the larger particles rise above the smaller ones [7].

The radially averaged packing fractions as a function of height are shown in Fig. 4. The three curves correspond to the three relative fractions of component 1 and component 2. In all cases, the packing fraction of both components increases steeply at small heights, reaches a maximum, and decays at large heights. The packing fraction of component 1 decreases and it increases for component 2 as the relative amount of each component is changed. The changes in the relative fractions only affect the magnitudes of the packing fractions. There is no noticeable variation in the details of the packing fraction profiles (i.e., the position of the maximum, the rate of decay, etc.) as the relative amounts of the components are changed.

3. Temperature

The granular temperature of each component is also studied as a function of the relative proportions. Figure 5 shows contour plots of the granular temperature of component 1 in the *x* [Fig. 5(a)], *y* [Fig. 5(b)], and *z* [Fig. 5(c)] directions for the system presented in Fig. 2. The symmetry evident in the *x* and *y* directions is produced by the unbiased introduction of energy into these directions by particle-particle collisions. These two partial temperatures decay rapidly in both the radial and vertical dimensions from a maximum near the center of the cylinder, close to the vibrating base. The *z* direction, however, is different because of the bias introduced by the vibrating base. This partial temperature decays in the vertical dimension with very little radial dependence at small heights. At larger heights, the center of the cylinder is slightly warmer than the surrounding area, as would be expected given the toroidal flow profile presented in Fig. 2.

Figure 6 shows the height dependence of the radially averaged, partial granular temperatures of each component. It can be seen that the height profiles of the temperature are similar for both components at all relative proportions. The temperatures in the *x* and *y* directions show the formation of a maximum for both components as height increases. These maxima occur very close to the height that corresponds to the maximum in packing fraction. The increase in the partial temperatures can then be attributed to an increase of particle-particle collisions that inject energy into the *x* and *y* directions, increasing the corresponding temperatures. Figure 6 also shows that the temperature in the *z* direction is larger than that in the other two directions. The minimum observed as height increases has been predicted by Brey *et al.* for systems in which the particles do not interact with a top barrier, but are under the influence of gravity [31]. Wildman *et al.* observed the minimum in the experimental systems [30,32], and Ramirez and Soto presented a hydrodynamic theory that addresses this phenomenon [33].

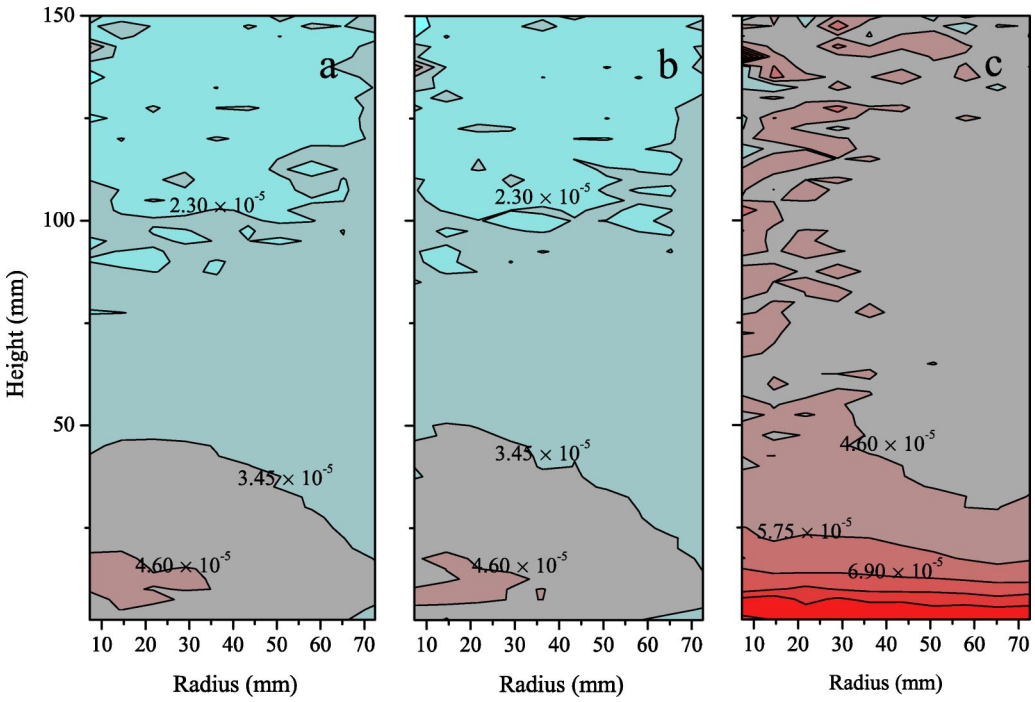

FIG. 5. (Color online) Contour plots of the temperature in the (a) x direction, (b) y direction, and (c) z direction for component 1. Contours correspond to a change of 11.5 μJ. Simulation conditions as given in Fig. 2.

Figures 6(a) and 6(b) also show that the temperatures of the two components change as the relative proportion of the two components changes. The temperature in the three spatial directions decreases as the relative proportion of the larger particles is decreased. As the fraction of component 1 decreases, the number of collisions with the smaller particles increases, causing the temperature of the larger particles to decrease. Also, the temperature of the entire system decreases because component 2 does not gain as much kinetic energy from the base since it is lighter than component 1. The decrease in the temperature, however, does not change the height at which the extrema in T_x, T_y, and T_z are observed. Only the magnitude of the measured temperature appears to change in these systems [Figs. 6(a) and 6(b)].

While the trends observed in the temperature of the two components are similar, there are differences between the two components. The temperatures of component 1 [Fig. 6(a)] are greater than those of component 2 [Fig. 6(b)] in all the systems, an effect particularly pronounced in the z direction. The temperatures in the x and y directions differ only slightly. It is difficult to determine whether the differences in temperature between the two components are dominated by the differences in size or mass from these data. Thus, we conducted further simulations to determine the individual effects of mass and size.

B. Systems with varying mass ratio

To determine the effects of particle mass, we simulated systems with mass ratios $m_2/m_1=0.01$, 0.125, 0.25, 0.5, and 1.0 at constant size, $d_2/d_1=1.0$, and relative fraction $n_2/n_1=1.0$ and with a total $n_1+n_2=1050$ particles in the system.

1. Energy distribution

We expect changes in the mass ratio to affect the exchange of energy, and hence the temperature, of each component. We therefore computed the average change in energy, $\langle \Delta E_\alpha \rangle_\beta$, of a particle of component α resulting from collisions with particles of component β. We examined the energy exchanges resulting from particle-particle, particle-wall, and particle-base collisions. The data we collected from the simulations for each kind of collision are presented in Fig. 7.

As expected, both components lose energy on collision with the wall, while they experience a net energy gain on collision with the base [Fig. 7(a)]. Both components also lose energy from intracomponent, particle-particle collisions [squares in Fig. 7(b)]. The intercomponent, particle-particle collisions [circles in Fig. 7(b)], however, show trends that are not intuitively obvious. Component 1 shows a loss of energy for all mass ratios, while component 2 shows that there may be a loss or gain of energy depending on the mass ratio. We obtained a theoretical estimate for this quantity by assuming each component has a Maxwell-Boltzmann velocity distribution but with a temperature specific to the component. The details of the derivation are presented in the Appendix. The average energy loss for a particle of component α resulting from collisions with particles of component β and average component temperatures (kinetic energies) of T_α and T_β is

$$\langle \Delta E_\alpha \rangle_\beta = k_B \mu (1+c) \left((1+c) \frac{T_\beta m_\alpha + T_\alpha m_\beta}{m_\alpha (m_\alpha + m_\beta)} - 2 \frac{T_\alpha}{m_\alpha} \right), \tag{7}$$

where k_B is the Boltzmann constant. The total average en-

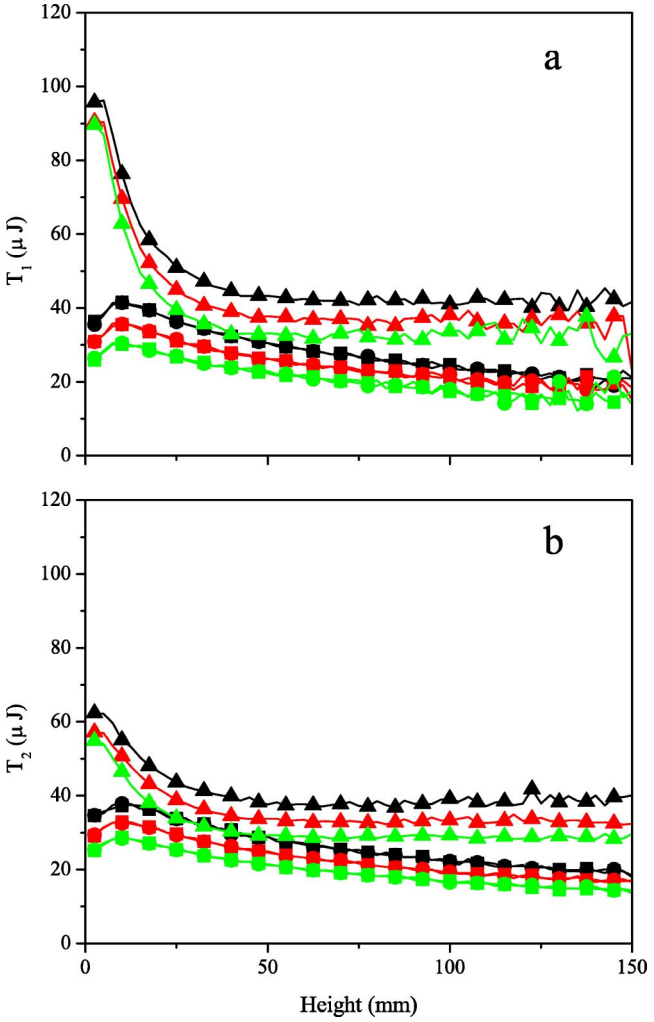

FIG. 6. (Color online) Temperatures in the x (■), y (●), and z (▲) directions of (a) component 1 and (b) component 2. The three spacial directions are shaded the same for each system. Simulation conditions as follows: $n_1=525$, $n_2=270$ (top curves); $n_1=350$, $n_2=540$ (middle curves); $n_1=175$, $n_2=810$ (bottom curves).

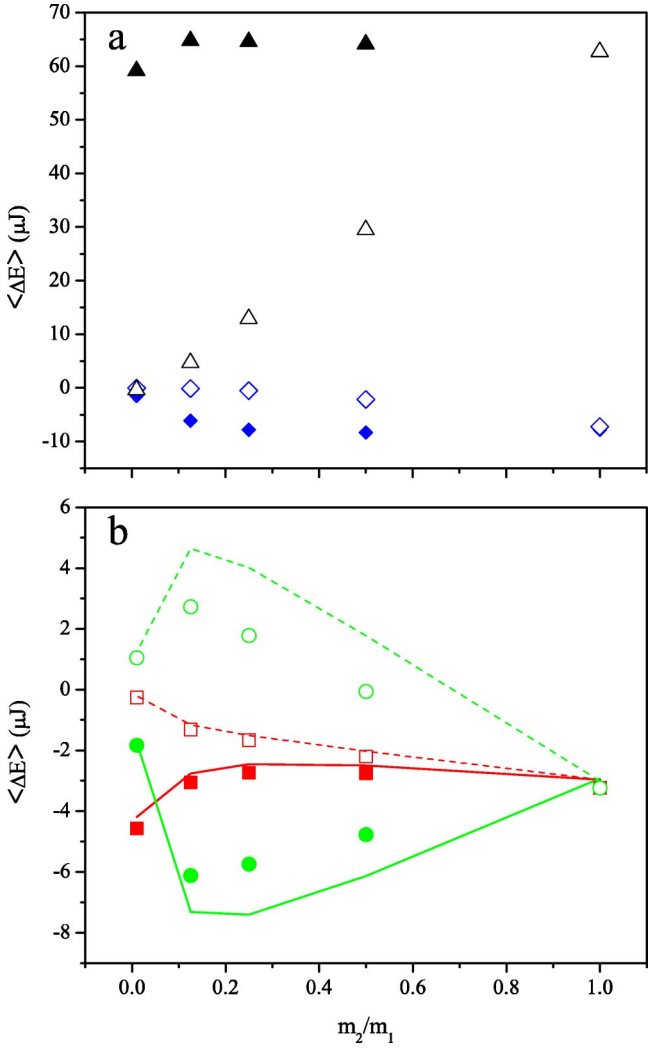

FIG. 7. (Color online) Average energy change per particle per collision for (a) particle-boundary collisions and (b) particle-particle collisions as the mass ratio is changed. Component 1 is represented by the closed symbols and component 2 is represented by the open symbols. The different kinds of collisions are: ■, intracomponent, particle-particle ($\langle\Delta E_1\rangle_1$ and $\langle\Delta E_2\rangle_2$); ●, intercomponent, particle-particle ($\langle\Delta E_1\rangle_2$ and $\langle\Delta E_2\rangle_1$); ♦, particle-wall, and ▲, particle-base. The solid (dashed) lines are the energy loss for component 1 (component 2) as calculated by Eq. (7) for intracomponent (same shade as the squares) and intercomponent (same shade as the circles), particle-particle collisions.

ergy loss per collision between particles of components α and β with temperatures of T_α and T_β is

$$\langle\Delta E_\alpha\rangle_\beta+\langle\Delta E_\beta\rangle_\alpha=-k_B(1-c^2)\frac{T_\beta m_\alpha+T_\alpha m_\beta}{m_\alpha+m_\beta}. \quad (8)$$

Equation (8) indicates that for inelastic collisions, $c<1$, the total energy of the colliding pair always decreases, even if the temperatures of the two components are different. For equal temperatures, Eq. (7) shows that this is also true for the individual energies of the components. If, however, the temperatures are different, it is possible for the energy of the lighter component to *increase* on average due to collisions with the heavier component.

We calculated values of $\langle\Delta E_\alpha\rangle_\beta$ for intercomponent and intracomponent, particle-particle collisions for each component using Eq. (7). The masses of the particles and the restitution coefficient are set by the input parameters, but the temperatures of each component are not known *a priori*. Therefore, the temperature was obtained from the simulation output for each mass ratio. The results from Eq. (7) are presented in Fig. 7(b) along with the results obtained from the simulation. It can be seen that the average energy changes calculated for the two kinds of particle-particle collisions compare favorably with those obtained from the simulation. There is better agreement for intracomponent collisions because there is no temperature or mass difference between the colliding particles. The predicted energy changes for intercomponent collisions show the same trend that is observed in the simulation results, but the magnitude of the change is incorrect. Specifically, the equation overestimates the change in energy resulting from intercomponent, particle-particle

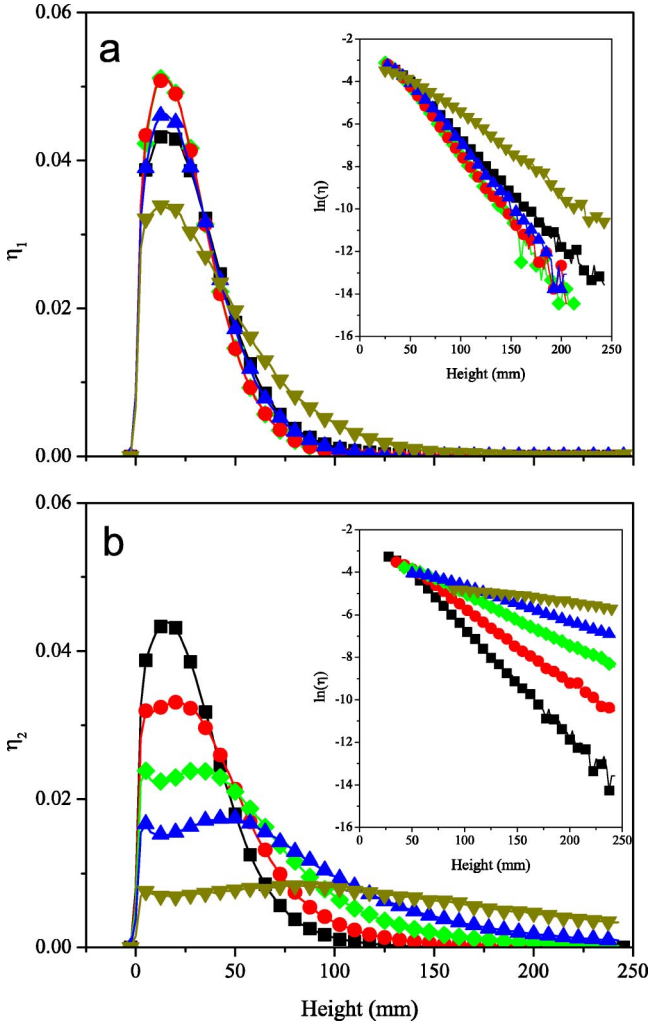

FIG. 8. (Color online) Packing fraction of (a) component 1 and (b) component 2 for mass ratios of ■, $m_2/m_1=1.0$, ●, $m_2/m_1=0.5$; ♦, $m_2/m_1=0.25$; ▲, $m_2/m_1=0.125$; and ▼, $m_2/m_1=0.01$. All other simulation parameters are as given in the text. The inset shows the natural log of the trailing edge of the packing fraction for each system.

collisions. This error probably arises from the inhomogeneities in the particle density and temperature (see Figs. 3 and 5), which are not accounted for in the Maxwell-Boltzmann distribution.

More generally, we note that as the mass ratio decreases, the energy change associated with any collision also decreases. This variation in the energy change will affect the bulk properties observed for these systems, such as the packing fraction and the temperature discussed below.

2. Packing fraction

The packing fraction of each component as a function of height is presented in Fig. 8. The general behavior is the same for both components, and is similar to that already discussed in Sec. III A 2. The packing fraction of component 1 varies little with mass ratio changes. In particular, the maximum density is at the same height for all the systems examined. At greater heights, however, component 1 condenses and then expands as the mass of component 2 decreases. This phenomenon is more clearly visible in the inset of Fig. 8(a), which shows a linear relationship between $\ln(\eta)$ and the height. At large altitudes, the slopes of the lines in the inset increase as component 1 condenses and decrease as component 1 expands in the system. This behavior corresponds to the increased energy loss that is observed for intercomponent, particle-particle collisions (see Fig. 7).

The packing fraction profiles of component 2 undergo a much more significant change as the mass ratio is decreased. Specifically, Fig. 8(b) indicates a steady depletion of this component from around the maximum, with a compensating increase at large altitudes, as the particles expand into the upper reaches of the cylinder. For mass ratios of 0.25 and below, two local maxima are present. These are most distinct for the systems in which component 2 has a net gain in energy due to collisions with particles of component 1 (mass ratios of 0.125 and 0.01). Thus, the two maxima are formed as the particles of component 2 try to separate from component 1. The increase in the energy forces the particles of component 2 toward the base and toward higher altitudes. This is what is observed in the packing fractions shown in Fig. 8(b) with one maximum very close to the base, and one maximum that increases in altitude as the mass ratio decreases. The plots of $\ln(\eta)$, shown in the inset, display a steady decrease in the slope as the mass ratio decreases.

3. Temperature

The effect of mass ratio on the temperature in the z direction for components 1 and 2 is shown in Figs. 9(a) and 9(b), respectively. The minimum in the temperature is obvious for both particles. It is also easily seen that the temperature in the z direction of component 1 goes through a minimum as the mass ratio of the two components decreases. The temperatures in the x and y directions (not shown) also follow the same trend. This indicates that total temperature for component 1 goes through a minimum as the mass ratio is decreased. The changes in the temperature coincide with the changes observed in the packing fraction [Fig. 8(a)] and the energy changes for the different kinds of collisions (Fig. 7). This implies that the changes in the velocities of the particles of component 1 affect the temperature, just as expected from Eqs. (6). As shown by Brey *et al.* [31] and Warr *et al.* [34], a relationship exists between the temperature and the packing fraction in a single component system. Extending their results to a multicomponent system, we obtain

$$\frac{d\ln(\eta_\alpha)}{dz} \sim -\frac{m_\alpha g}{k_B T_\alpha}. \tag{9}$$

This equation holds for high altitudes and restitution coefficients close to 1. Thus, a limiting temperature can be calculated for each system using the data presented in the inset of Fig. 8(a). The results, plotted as horizontal lines in Fig. 9(b), correspond well with the asymptotic temperatures. This indicates that the decaying edge of the packing fraction is a good indicator of the temperature at those altitudes.

We observed trends for component 2 that are very different from those just discussed for component 1. Figure 9(b)

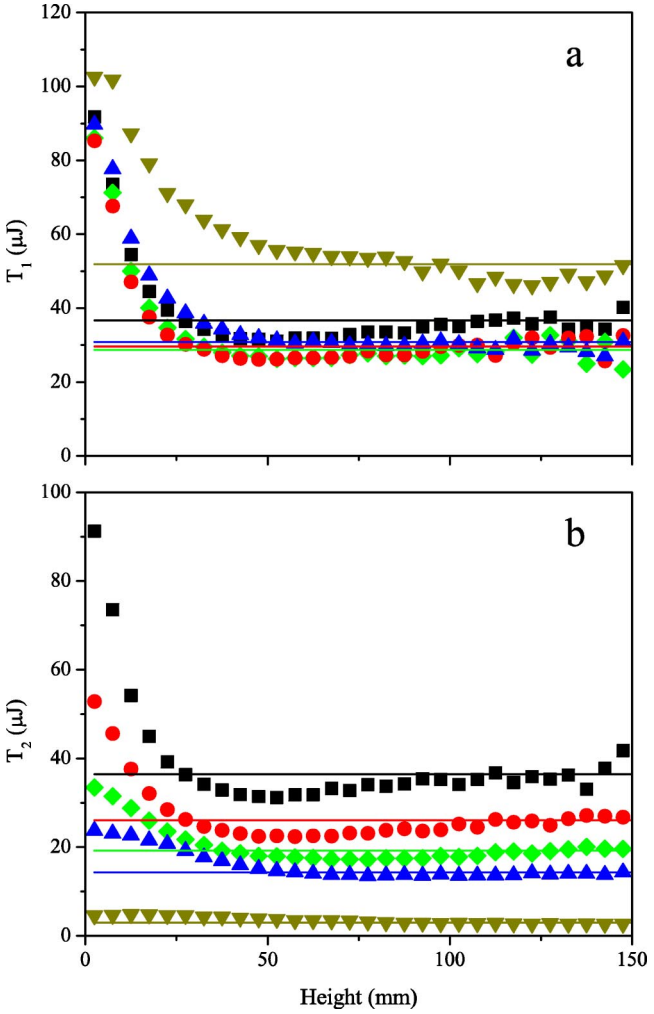

FIG. 9. (Color online) The temperature in the z direction of (a) component 1 and (b) component 2 for mass ratios of ■, $m_2/m_1=1.0$; ●, $m_2/m_1=0.5$; ♦, $m_2/m_1=0.25$; ▲, $m_2/m_1=0.125$; and ▼, $m_2/m_1=0.01$. The temperature calculated from Eq. (9) is shown as a line corresponding to the data points of the same shade.

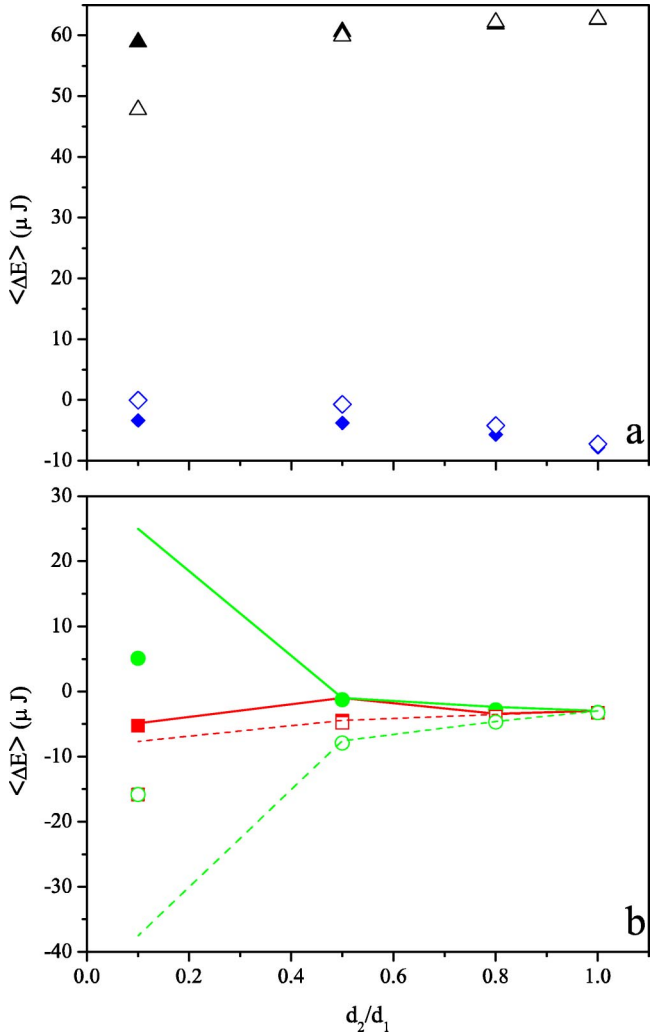

FIG. 10. (Color online) Average energy change per particle per collision for (a) particle-boundary collisions and (b) particle-particle collisions as the size ratio is changed. Component 1 is represented by the closed symbols and component 2 is represented by the open symbols. The different kinds of collisions are: ■, intracomponent, narticle-particle ($\langle\Delta E_1\rangle_1$ and $\langle\Delta E_2\rangle_2$); ●, intercomponent, particle-particle ($\langle\Delta E_1\rangle_2$ and $\langle\Delta E_2\rangle_1$); ♦; particle-wall; and ▲; particle-base. The solid (dashed) lines are the energy loss for component 1 (component 2) as calculated by Eq. (7) for intracomponent (same shade as the squares) and intercomponent (same shade as the circles), particle-particle collisions.

shows that the temperature decreases as the mass ratio decreases. The decrease is expected since temperature is directly related to the mass of the particle [Eqs. (6)]. Thus, the lighter particles will have a lower temperature than the heavier particles. Component 2 exhibits a minimum as the height increases, just as in the case of component 1. However, the minimum becomes shallower as the temperature decreases. Figure 9(b) also shows the temperature obtained from the packing fraction using Eq. (9). Again, we find that there is good agreement between the temperature calculated by Eq. (9) and that calculated from Eqs. (6) for large heights.

C. Effect of varying size ratio

Finally, we studied the effects of particle size by simulating systems with size ratios of $d_2/d_1=1.0$, 0.8, 0.5, and 0.1. The mass ratio was held constant at $m_2/m_1=1.0$, and the relative fraction was held constant at $n_2/n_1=1.0$, with $n_1+n_2=1050$. The changes observed in the energy distributions, the packing fraction, and the partial temperatures are presented and discussed below.

1. Energy distribution

Changes in particle size result in changes in the mean free path [31] and the pair correlation function at contact [10,14,15]. These changes affect the particle velocities by changing the number of collisions that a particle experiences in a given amount of time. Thus, changes in the size ratio are expected to result in changes in the distribution of the energy, just as observed for the mass ratio.

Figures 10(a) and 10(b) show the average energy changes that particles of components 1 and 2 experience as a result of

collision. Collisions with the wall cause a loss of energy for both components while collision with base increases the energy of the particles for all size ratios [Fig. 10(a)]. The collisions between particles, however, show different trends than seen in the mass ratio study. As seen in Fig. 10(b), the intercomponent collisions do not result in an energy loss for component 1 for all size ratios. The smaller the size ratio, the greater the amount of energy injected per collision into component 1 from collisions with component 2. All particle-particle collisions decrease the energy of component 2. The energy loss per collision for both intercomponent and intracomponent, particle-particle collisions increases as the size ratio decreases. It is interesting to note that the energy loss due to both intercomponent and intracomponent collisions is the same for component 2 at the smallest size ratio. The energy changes for all but the smallest size ratio agree well with those predicted by Eq. (7). The smallest size ratio shows a large deviation between the energy loss predicted by the equations and that determined from the simulation. One reason for the discrepancy is the assumption of Maxwell-Boltzmann velocities used in determining the equations. The differences in the distribution of energy within each component and between the two components that we observe here will affect the packing fraction and temperature for these systems.

2. Packing fraction

Figure 11 shows the effect of the size ratio on the packing fraction of the system. We can see that component 1 reaches higher altitudes as the diameter of component 2 decreases without any noticeable shift in the position of the maximum in packing fraction. This implies that the particles of component 1 expand through the system as the size ratio decreases. There are two possible causes of the increase in the tail of the packing fraction at large heights. First, the particles of component 1 are able to retain more energy because of a decrease in the collision rate between particles as the size ratio decreases. The decrease in the collision rates is the result of a decrease in the total excluded volume of the system as the size of component 2 is reduced [deduced from Figs. 11(a) and 11(b)]. The change in the total excluded volume of the system reduces the amount of energy lost to particle-particle collisions. The other cause of the increased altitude is the energy gain that comes from collisions with component 2. Since energy can be gained at positions above the base, the particles will be able to travel to higher altitudes in the system.

Figure 11(b) shows the effect of the size ratio on component 2. We can see an overall reduction in the packing fraction of component 2 as the particle size is reduced. This occurs because the number of particles of component 2 is held fixed as the size is decreased. We also see that the particles of component 2 are able to reach greater altitudes in the system as the size ratio decreases [see the inset in Fig. 11(b)]. The increase in the altitude is the result of the decrease in the number of collisions discussed above.

3. Temperature

Figure 12(a) shows the z component of the granular temperature as a function of height for component 1 for the four

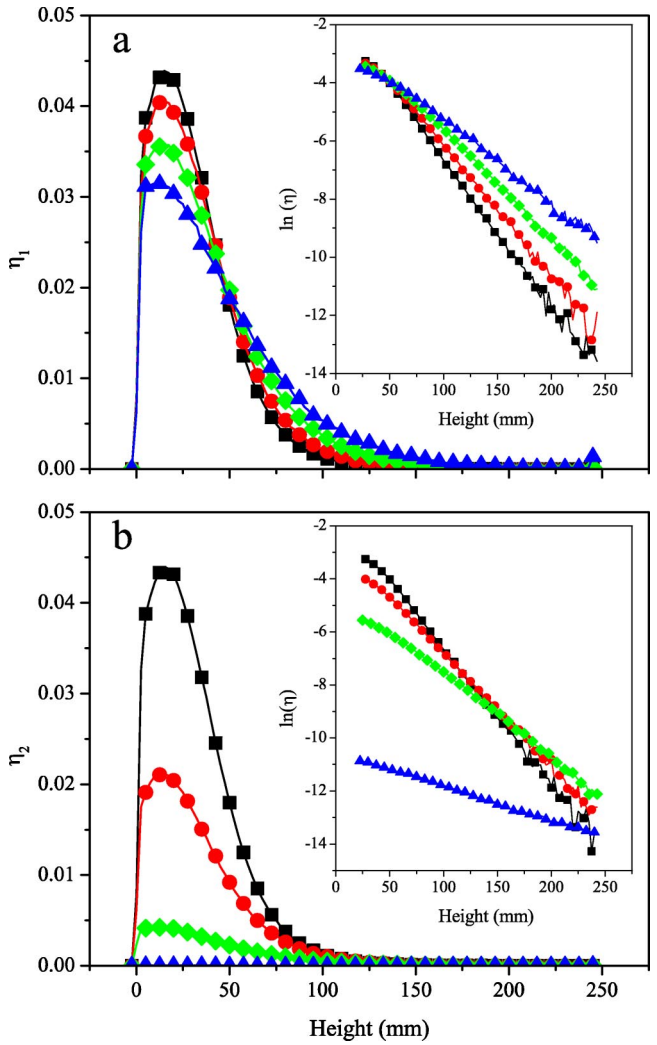

FIG. 11. (Color online) The packing fraction of (a) component 1 and (b) component 2 for size ratios of ■, $d_2/d_1=1.0$; ●, $d_2/d_1=0.8$; ◆, $d_2/d_1=0.5$; and ▲, $d_2/d_1=0.1$. All other simulation parameters are as given in the text. The inset shows the natural log of the trailing edge of the packing fraction for each system.

size ratios. Figure 12(b) shows the same for component 2 of the mixture. A minimum is again observed in the temperatures of each system for each component. The other general features of the temperature profiles in the x and y directions, while not shown here, are the same as seen and discussed in connection with Fig. 6. It can be easily seen in Fig. 12 that the temperatures of both the large and small particles increase as the size ratio decreases. This increase in temperature results from a decrease in the energy lost due to particle-particle collisions. The reduction in the collision rate as the size ratio decreases can be observed in Table I. It is interesting that the energy loss due to intracomponent collisions increases for component 2 as the collision rate for intracomponent collisions decreases [Figure 10(b)]. In addition, there is a discrepancy between the theory and the simulation results observed in Fig. 10 at small size ratios that should be noted. The deviations are the result of the systems being dominated by collisions with the wall and not particle-particle collisions (see Table I), as assumed in the theory (see the Appendix).

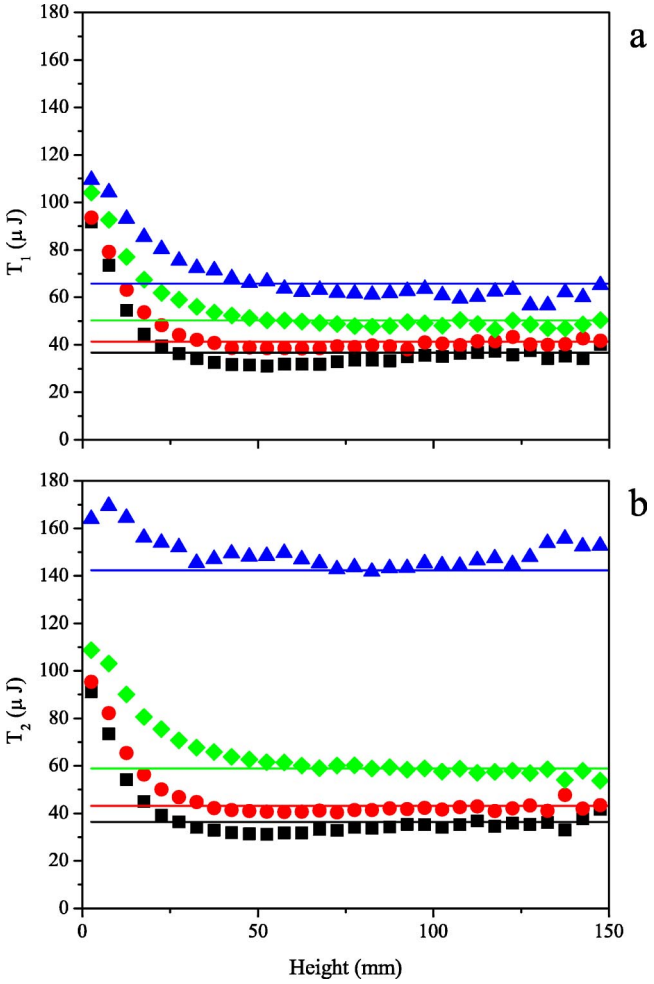

FIG. 12. (Color online) The temperature in the z direction of (a) component 1 and (b) component 2 for size ratios of ■, $d_2/d_1=1.0$; ●, $d_2/d_1=0.8$; ♦, $d_2/d_1=0.5$; and ▲, $d_2/d_1=0.1$. The temperature calculated from Eq. (9) is shown as a line corresponding to the data points of the same shade.

We used Eq. (9) and the high altitude tails of the packing fractions shown in the insets in Figs. 11(a) and 11(b) to calculate a temperature. The temperatures calculated in this manner are also plotted in Fig. 12. The temperature calculated from Eq. (9) coincides with the temperature in the z direction at large heights, just as in the case of the mass ratio. The agreement between the two temperatures is very good for both components for each size ratio, except the smallest. This may indicate that the packing fraction is not a very sensitive measure of the temperature when the difference in size between the components is large. The difference in the two temperatures may also be indicative of the changes in the dominant processes in the energy distribution. For example, the smallest size ratio is not dominated by particle-particle collisions like the other systems. The edge effects associated with the walls of the cylinder become more important, but they are not considered in the theory used to obtain Eq. (9).

IV. CONCLUSIONS

We have shown that, like the single component system [18], the simulation results reproduce the phenomena observed in experimental studies. Specifically, the experimentally observed [17] flow pattern, radial dependence of the packing fraction, and temperature of the two components are qualitatively reproduced by the simulation.

There are a number of possible reasons for the quantitative differences between the simulation and experiments. For example, for each component the simulated particles are identical spheres, while in the experimental system there is a small distribution of shape, size, and mass. The simulation also assumes that the particles are frictionless with constant restitution coefficients, which is not the case for ballotini glass spheres used in the experiments. The sawtooth wave form of the vibrating base is an idealization of the sinusoidal vibration of the experiment. It is thought, however, that this does not have a large influence on the system behavior [25]. In any case, we feel confident that our model captures the key physical aspects of the experimental system and can therefore be used to study the influence of various system parameters.

We also studied the effects of mass and size ratio in this paper. Generally, we observed that changes in either ratio do not result in any segregation of the particles. The lighter particles attain greater heights than the heavier particles in the mass ratio studies. For both components the rate of decay of the packing fraction at large heights is a good indication of the granular temperature in that region [31,34].

As the mass ratio decreases, the overall temperature of the system decreases. This is consistent with the lower amount of energy gained by the lighter component from the vibrating base and an overall lowering of the efficiency of energy transfer as the mass ratio decreases. The packing fraction and temperature of the individual components, however, have a nontrivial dependence on the mass ratio. For the heavier component, both these quantities exhibit a minimum as the

TABLE I. Collision rates (s^{-1}) for the different kinds of collisions for components 1 and 2.

	Component 1				Component 2			
Size ratio	Intracomponent	Intercomponent	Wall	Base	Intracomponent	Intercomponent	Wall	Base
1.0	272.8	546.2	181.2	78.8	272.1	546.2	195.1	78.8
0.8	252.4	412.0	278.5	74.7	164.1	412.0	381.2	77.1
0.5	230.0	248.1	503.0	70.3	55.2	248.1	2587.4	71.9
0.1	208.9	72.5	649.4	68.1	7.75	72.5	136 270	54.4

mass ratio decreases. We also observed that the energy changes due to intercomponent collisions exhibit extrema for each component as the mass ratio decreases. Specifically, the heavier component shows a minimum, whereas the lighter component shows a maximum in the energy change. The lighter component actually gains energy from collisions with the other component around a mass ratio of $m_2/m_1=0.5$. The energy changes due to intracomponent collisions for both components, however, are negative for all mass ratios. The energy loss due to intraparticle collisions increases for the heavy component as the mass ratio decreases, while it decreases for the lighter component. For comparison, we developed an approximate theory to calculate the energy changes for particle-particle collisions by assuming that the particle velocities follow a Maxwell-Boltzmann distribution with a component specific temperature. While this assumption is not strictly correct given the inhomogeneities in density and temperature, the theory is qualitatively accurate for the intercomponent collisions and in near quantitative agreement with the simulation for the intracomponent collisions.

As the size ratio decreases at constant mass ratio, the overall temperature of the system increases and the total packing fraction decreases. The particle-particle and particle-boundary collision rates decrease and increase, respectively, as the size ratio decreased. At the same time, the larger particles begin to gain energy from collisions with the smaller component. The approximate theory of the energy changes is again able to reproduce qualitatively the observed trends. However, the agreement between the theory and simulation results worsens as the size ratio decreases.

Wildman and Parker [17] observed a decrease in the temperature as they decreased the ratio of the number of large to small ballotini spheres. Our results show that this effect is dominated by the difference in mass of the two components, and not the difference in size.

ACKNOWLEDGMENTS

We thank Ricky Wildman for useful discussions and the National Science Foundation (Grant No. CHE-9814236) for financial support.

APPENDIX: ENERGY DISSIPATION EQUATIONS

The energy change of particle i of component α resulting from collision with particle j of component β is

$$2m_\alpha \Delta E_{\alpha,i}=\mu^2(1+c)^2(\mathbf{v_{ij}}\cdot\hat{\mathbf{n}})^2-m_\alpha\mu(1+c)\times[(\mathbf{v_{\alpha,i}}\cdot\hat{\mathbf{n}})^2-(\mathbf{v_{\beta,j}}\cdot\hat{\mathbf{n}})^2+(\mathbf{v_{ij}}\cdot\hat{\mathbf{n}})^2], \quad \text{(A1)}$$

where $\mathbf{v_{ij}}=\mathbf{v_{\alpha,i}}-\mathbf{v_{\beta,j}}$ and $\mu=m_\alpha m_\beta/(m_\alpha+m_\beta)$. The total energy loss due to the collision is simply $\Delta E_{total}=\Delta E_{\alpha,i}+\Delta E_{\beta,j}$, or

$$\Delta E_{total}=-\frac{1}{2}\mu(1-c^2)(\mathbf{v_{ij}}\cdot\hat{\mathbf{n}})^2. \quad \text{(A2)}$$

These equations are exact for each collision that occurs in the system. In order to determine the average values, however, some assumptions must be made. Specifically, we assume that the velocities of each component are described by a Maxwell-Boltzmann distribution that is homogeneous, isotropic, and characterized by a component-specific temperature T_α,

$$f(\mathbf{v_{\alpha,i}})d\mathbf{v_{\alpha,i}}=\left(\frac{2\pi m_\alpha}{k_BT_\alpha}\right)^{3/2}\exp\left(-\frac{m_\alpha v_{\alpha,i}^2}{2k_BT_\alpha}\right)d\mathbf{v_{\alpha,i}}. \quad \text{(A3)}$$

In order to average over the velocities $\mathbf{v_{\alpha,i}}$, $\mathbf{v_{\beta,j}}$, and $\mathbf{v_{ij}}$ appearing in Eqs. (A1) and (A2), we introduce center of mass $\mathbf{v_c}$, and relative $\mathbf{v_r}$ velocities:

$$\mathbf{v_{\alpha,i}}=\frac{m_\beta/T_\beta}{m_\alpha/T_\alpha+m_\beta/T_\beta}\mathbf{v_r}+\mathbf{v_c}, \quad \text{(A4)}$$

$$\mathbf{v_{\beta,j}}=-\frac{m_\alpha/T_\alpha}{m_\alpha/T_\alpha+m_\beta/T_\beta}\mathbf{v_r}+\mathbf{v_c}, \quad \text{(A5)}$$

$$\mathbf{v_{ij}}=\mathbf{v_{\alpha,i}}-\mathbf{v_{\beta,j}}=\mathbf{v_r}. \quad \text{(A6)}$$

In this coordinate system the energy change for particle i becomes

$$2m_\alpha\Delta E_{\alpha,i}=\mu^2(1+c)^2(\mathbf{v_r}\cdot\hat{\mathbf{n}})^2-2T_\alpha\mu'\mu(1+c)(\mathbf{v_r}\cdot\hat{\mathbf{n}})^2-2m_\alpha\mu(1+c)(\mathbf{v_r}\cdot\hat{\mathbf{n}})(\mathbf{v_c}\cdot\hat{\mathbf{n}}), \quad \text{(A7)}$$

where

$$\mu'=\frac{(m_\alpha/T_\alpha)(m_\beta/T_\beta)}{m_\alpha/T_\alpha+m_\beta/T_\beta}. \quad \text{(A8)}$$

The total energy loss [shown in Eq. (A2)] becomes

$$\Delta E_{total}=-\frac{1}{2}\mu(1-c^2)(\mathbf{v_r}\cdot\hat{\mathbf{n}})^2 \quad \text{(A9)}$$

in the new coordinate system.

It is now necessary to average Eqs. (A7) and (A9) over the fraction of collisions between a particle of component α with a particle of component β with a relative velocity between v_r and v_r+dv_r. Straightforward modification of the standard kinetic theory result [35] gives

$$p(v_r)dv_r=\frac{1}{2}\left(\frac{\mu'}{k_B}\right)^2v_r^3\exp\left(-\frac{\mu'v_r^2}{2k_B}\right)dv_r. \quad \text{(A10)}$$

We then compute

$$\langle(\mathbf{v_r}\cdot\hat{\mathbf{n}})^2\rangle=\int_0^\infty dv_r p(v_r)\int_0^\sigma db\,h(b)(\mathbf{v_r}\cdot\hat{\mathbf{n}})^2, \quad \text{(A11)}$$

where $h(b)db=(2b/\sigma^2)db$ is the probability that the impact parameter lies between b and $b+db$. Substituting $(\mathbf{v_r}\cdot\hat{\mathbf{n}})^2=v_r^2(1-(b/r)^2)$ and evaluating the integrals leads to

$$\langle(\mathbf{v_r}\cdot\hat{\mathbf{n}})^2\rangle=\frac{2k_B}{\mu'}. \quad \text{(A12)}$$

Using this result and the fact that $\langle(\mathbf{v_r}\cdot\hat{\mathbf{n}})(\mathbf{v_c}\cdot\hat{\mathbf{n}})\rangle=0$ gives Eqs. (7) and (8).

[1] S. Douday, S. Fauve, and C. Laroche, Europhys. Lett. **8**, 621 (1989).
[2] H.K. Pak and R.P. Behringer, Phys. Rev. Lett. **71**, 1832 (1993).
[3] F. Melo, P.B. Umbanhowar, and H.L. Swinney, Phys. Rev. Lett. **75**, 3838 (1995).
[4] P.B. Umbanhowar, F. Melo, and H.L. Swinney, Nature (London) **382**, 793 (1996).
[5] P. Evesque and J. Rajchenbach, Phys. Rev. Lett. **62**, 44 (1989).
[6] E.E. Ehrichs, H.M. Jaeger, G.S. Karczmar, J.B. Knight, V.Y. Kuperman, and S.R. Nagel, Science **267**, 1632 (1995).
[7] A. Rosato, K.J. Shandburg, F. Prinz, and R.H. Swendsen, Phys. Rev. Lett. **58**, 1038 (1987).
[8] W. Losert, D.G.W. Cooper, J. Delour, A. Kudrolli, and J.P. Gollub, Chaos **9**, 682 (1999).
[9] S. McNamara and S. Luding, Phys. Rev. E **58**, 2247 (1998).
[10] V. Garzo and J. Dufty, Phys. Rev. E **60**, 5706 (1999).
[11] S.R. Dahl, C.M. Hrenya, V. Garzo, and J.W. Dufty, e-print cond-mat/0205413.
[12] U.M.B. Marconi and A. Puglisi, Phys. Rev. E **65**, 051305 (2002).
[13] U.M.B. Marconi and A. Puglisi, Phys. Rev. E **66**, 011301 (2002).
[14] A. Barrat and E. Trizac, Granular Matter **4**, 57 (2002).
[15] A. Barrat and E. Trizac, e-print cond-mat/0207267.
[16] K. Feitosa and N. Menon, e-print cond-mat/0111391.
[17] R.D. Wildman and D.J. Parker, Phys. Rev. Lett. **88**, 064301 (2002).
[18] J. Talbot and P. Viot, Phys. Rev. Lett. **89**, 064301 (2002).
[19] D. Paolotti, C. Cattuto, U.M.B. Marconi, and A. Puglisi, e-print cond-mat/0207601.
[20] T. Pöschel, T. Schwager, and C. Salueña, Phys. Rev. E **62**, 1361 (2000).
[21] A. Barrat and E. Trizac, e-print cond-mat/0207267.
[22] R. Pagnani, U.M.B. Marconi, and A. Puglisi, Phys. Rev. E **66**, 051304 (2002).
[23] R. Clelland and C.M. Hrenya, Phys. Rev. E **65**, 031301 (2002).
[24] J.A.C. Gallas, H.J. Herrmann, T. Pöschel, and S. Sokolowski, J. Stat. Phys. **82**, 443 (1996).
[25] S. McNamara and J.L. Barrat, Phys. Rev. E **55**, 7767 (1997).
[26] A. Barrat, E. Trizac, and J.N. Fuchs, Eur. Phys. J. E **5**, 161 (2001).
[27] N.V. Brilliantov, F. Spahn, J.M. Hertzsch, and T. Pöschel, Phys. Rev. E **53**, 5382 (1996).
[28] D. Goldman, M.D. Shattuck, C. Bizon, W.D. McCormick, J.B. Swift, and H.L. Swinney, Phys. Rev. E **57**, 4831 (1998).
[29] S. Luding and S. McNamara, e-print cond-mat/9810009.
[30] R.D. Wildman, J.M. Huntley, and D.J. Parker, Phys. Rev. Lett. **86**, 3304 (2001).
[31] J.J. Brey, M.J. Ruiz-Montero, and F. Moreno, Phys. Rev. E **63**, 061305 (2001).
[32] R.D. Wildman, J.M. Huntley, and D.J. Parker, Phys. Rev. E **63**, 061311 (2001).
[33] R. Ramirez and R. Soto, e-print cond-mat/0210471.
[34] S. Warr, J.M. Huntley, and G. Jacques, Phys. Rev. E **52**, 5583 (1995).
[35] D.A. McQuarrie, *Statistical Mechanics* (Harper & Row, New York, 1976), Chaps. 7 and 16.